

DOI 10.24425/ae.2024.149917

Development of an emulation platform for synchronous machine power generation system using a nonlinear functional level model

FILIP KUTT¹, ŁUKASZ SIENKIEWICZ¹✉, SZYMON RACEWICZ²,
MICHAŁ MICHNA¹, ROLAND RYNDZIONEK¹

¹*Gdańsk University of Technology, Faculty of Electrical and Control Engineering
ul. Gabriela Narutowicza 11/12, 80-233 Gdańsk, Poland*

²*University of Warmia and Mazury in Olsztyn, Faculty of Technical Science
ul. Oczapowskiego 11, 10-710 Olsztyn, Poland*

*e-mail: {filip.kutt/lukasz.sienkiewicz/michal.michna/roland.ryndzionek}@pg.edu.pl
szymon.racewicz@uwm.edu.pl,*

(Received: 18.08.2023, revised: 17.04.2024)

Abstract: The article presents the Power Hardware in the Loop (PHIL) approach for an autonomous power system analysis based on the synchronous generator model incorporating magnetic saturation effects. The model was prepared in the MATLAB/Simulink environment and then compiled into the C language for the PHIL platform implementation. The 150 kVA bidirectional DC/AC commercial-grade converter was used to emulate the synchronous generator. It was controlled by the real-time simulation control unit with the prepared synchronous generator model incorporating magnetic saturation effects. The proposed approach was validated on the 125 kVA synchronous generator connected to the active and reactive loads of different values for the steady-state and the transient-state performance studies.

Key words: autonomous power system, PHIL, power hardware in the loop, real-time modelling, synchronous generator

1. Introduction

This paper proposes an approach for implementing a nonlinear synchronous generator (SG) model in the power hardware in the loop (PHIL) emulation platform. The nonlinearity in the model is due to the incorporation of the magnetic saturation effect using the look-up table



© 2024. The Author(s). This is an open-access article distributed under the terms of the Creative Commons Attribution-NonCommercial-NoDerivatives License (CC BY-NC-ND 4.0, <https://creativecommons.org/licenses/by-nc-nd/4.0/>), which permits use, distribution, and reproduction in any medium, provided that the Article is properly cited, the use is non-commercial, and no modifications or adaptations are made.

method. The objective of the research was to develop a frequency converter (FC) based platform capable of emulating an autonomous power generation system. Unlike in nationwide power systems, where redundancy can ensure a reliable electrical energy supply [1], autonomous power generation systems are often the only solution for electric power supply in remote areas and are the only solution for onboard ships and airplane power delivery [1–4]. To maintain a high level of safety and reliability, tools that would allow real-time diagnosis need to be developed [5, 6]. An electromechanical energy converter in the form of an SG is a crucial component of such a system. The SG performance can influence the reliability and safety of the generation node itself and the reliability and safety of the other power system components (converters and loads) [7, 8]. The authors proposed a PHIL approach to investigate the influence of the SG output on the power system components. Such an approach should allow for the initial evaluation of the generator's performance as well as the influence of the generator's performance on the other power system components.

A significant challenge with power system emulation using PHIL is the required computational power for real-time simulation [9, 10]. For a given simulation platform, the minimum attainable time-step in the solver constrains the physical phenomena that can be represented faithfully. Amplifiers and I/O interfaces used in the PHIL simulation introduce delays and distortions, which further limit the frequency bandwidth of the whole platform [11, 12].

One of the solutions for mitigating the high computational requirement of the PHIL emulation platform is to use a commercially available FC instead of a purpose-built power amplifier (PA) as the high-power side of the PHIL emulation platform. Most commercial FCs are based on frequency inverters designed to control the speed of an electric motor. However, with an addition of an output LC or LCL filter (passive or active), such an inverter can be used as a PHIL high-power hardware component. In that case, the FC would emulate the operation of a switched-mode PA. The input variables are the most significant difference between the FC and the standard PA. In the proposed FC high-power component of the PHIL platform, the FC input variables are not instantaneous voltage or current values to be amplified but rather the set point of output voltage or current and the set point of output frequency [13]. The drawback in such operation conditions is the limited dynamic response of the PHIL emulation platform and the fact that the FC internal PID regulators limit this dynamic response [14]. The advantage is that this approach can provide adequate terminal waveform representation for the functional level analysis based on simulated RMS values. Most commercial-grade FCs can be paired with output filters with which this dynamic response can further be tuned to create a cost-effective alternative to purpose-built PAs.

In the PHIL platforms different interface algorithms (IAs) exist for the reference and feedback signals between the Real Time Simulator (RTS) and the high power side of the platform. The most common IA is the usage of an ideal transformer coupling. Other methods include partial circuit duplication, damping impedance, and modified damping impedance methods [13, 15]. The go-to method is the ideal transformer model for the IA, however, the PHIL instability issues might require using one of the other methods. Because the proposed approach to the PHIL emulation in this research is based on a functional level model and the FC takes the role of the high-power side of the platform, the ideal transformer model was used for the IA. This approach did not introduce significant instability issues in the emulation platform.

The objective of developing the PHIL emulation platform was to build a solution for multi-component autonomous power system emulation based on commercially available FCs. Because



of that, the research was not focused on the analysis of a single system component but instead on the performance impact of the component on the autonomous power system. Four modelling levels can be used to develop the SG model for the RTS (Fig. 1):

- At the architectural level, the models are usually used for power budget studying and do not allow for transient behaviour representation.
- At the functional level, the models are usually used for power system stability studies. Such models allow for the analysis of transient behaviour; however, the non-sinusoidal harmonic waveform analysis is impossible with these models.
- At the behavioural level, the models are usually used for network power quality studies. These models allow for both the transient state analysis and non-sinusoidal waveform analysis.
- The component level modelling is very similar to the behavioural level; however, all system components are subdivided, and the high-fidelity behavioural level models are used for all these subdivided components.

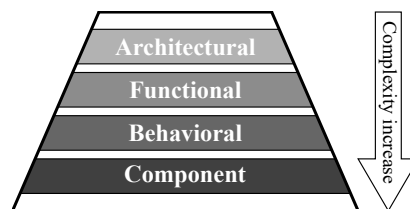


Fig. 1. Modelling complexity levels [16, 17]

The autonomous power generation system is characterized by the power level of the power generation node that can be of the same order as the power of a single load. This can lead to high-level dynamic load changes exerted on the SG during its normal operation. The control system can maintain fixed electrical parameters (voltage amplitude and frequency) in the steady state; however, those parameters can vary in transient states, including load changes and SG failures [7]. In order to represent the SG performance during the transient states, the authors propose the functional level model of the SG, which includes magnetic core saturation effects implemented in the RTS unit and the commercially available FC used as the PHIL emulation platform high-power component. The paper includes investigating the saturation effects on the system performance during the transient state operation. Therefore, the SG model used in the PHIL emulation platform will be subjected to sudden load changes that can occur in an autonomous power system.

The main objective of the research is to develop a platform capable of emulating the behaviour of a synchronous generator in an autonomous power system during high-load changes. In contrast to existing PHIL platforms that emulate the island operation of SGs, which propose a dedicated PA or specially designed voltage converters and closed platforms such as Typhoon HIL or dSpace [18, 19], the presented solution utilizes a commercially available frequency converter and a PC with industry-standard I/O interface as the PHIL platform.

The paper is organized as follows. Section 2 describes the development of the synchronous generator's discrete functional level model, including magnetic core saturation effects. Synchronous generator nonlinear model implementation using Matlab/Simulink is presented in Section 3. Section 4 explains the implementation of the model as a control algorithm for a commercially available

frequency converter and an off-the-shelf x64 PC as a real-time simulation platform. Moreover, verification of the PHIL platform by a comparative analysis using Simulink model implementation of an SG and measurements of the 125 kVA synchronous generator is given further in Section 4. The paper ends with conclusions on the performance of the proposed emulation platform.

2. Synchronous generator discrete model development

The main simplifications considered during the synchronous generator model development were:

- Single winding in direct and quadrature axes was used to represent damper winding.
- Saturation affects both the direct and quadrature axis in the same way.
- Self and mutual magnetizing inductances are affected by the saturation in the same way.

The model was developed using main voltage equations based on the SG model in an orthogonal $qd0$ reference frame and is defined as:

$$V_{qs}^r = -r_s i_{qs}^r + \omega_r \lambda_{ds}^r + \frac{d\lambda_{qs}^r}{dt}, \quad (1)$$

$$V_{ds}^r = -r_s i_{ds}^r + \omega_r \lambda_{qs}^r + \frac{d\lambda_{ds}^r}{dt}, \quad (2)$$

$$V_{0s}^r = -r_s i_{0s}^r + \frac{d\lambda_{0s}^r}{dt}, \quad (3)$$

$$0 = r'_{kq} i_{kq}^{rr} + \frac{d\lambda_{kq}^{rr}}{dt}, \quad (4)$$

$$0 = r'_{kd} i_{kd}^{rr} + \frac{d\lambda_{kd}^{rr}}{dt}, \quad (5)$$

$$V_{fd}^{rr} = r'_{fd} i_{fd}^{rr} + \frac{d\lambda_{fd}^{rr}}{dt}, \quad (6)$$

where: $V_{qs}^r, V_{ds}^r, V_{0s}^r$ are the armature voltages components in the $qd0$ reference frame, V_{fd}^{rr} is the excitation winding voltage, $i_{qs}^r, i_{ds}^r, i_{0s}^r$ are the armature currents in the $qd0$ reference frame, i_{fd}^{rr} is the excitation winding current, i_{kd}^{rr} is the current modelling the damper winding effects in the direct axis, i_{kq}^{rr} is the current modeling the damper winding effects in the quadrature axis, ω_r is the electrical angular velocity of the machine, $\lambda_{qs}^r, \lambda_{ds}^r, \lambda_{0s}^r$ are the armature winding flux linkages in the $qd0$ reference frame, λ_{fd}^{rr} is the excitation winding flux linkage, λ_{kd}^{rr} is the flux linkage modeling the damper winding effects in the direct axis and λ_{kq}^{rr} is the flux linkage modeling the damper winding effects in the quadrature axis. The superscript sign (') is used to denote the variables that are calculated for the armature winding number of turns and the r superscript is used to denote armature variables converted to the arbitrary synchronous rotating orthogonal reference frame $qd0$. The flux linkages are defined as:

$$\lambda_{qs}^r = -L_{ls} i_{qs}^r + k_{sat}^q L_{mq} (-i_{qs}^r + i_{kq}^{rr}), \quad (7)$$

$$\lambda_{ds}^r = -L_{ls} i_{ds}^r + k_{sat}^d L_{md} (-i_{ds}^r + i_{kd}^{rr} + i_{fd}^{rr}), \quad (8)$$

$$\lambda_{0s}^r = -L_{ls}i_{ds}^r, \quad (9)$$

$$\lambda_{kq}^{rr} = L'_{lkq}i_{kq}^{rr} + k_{\text{sat}}^q L_{mq} \left(-i_{qs}^r + i_{kq}^{rr} \right), \quad (10)$$

$$\lambda_{kd}^{rr} = L'_{lkd}i_{kd}^{rr} + k_{\text{sat}}^d L_{md} \left(-i_{ds}^r + i_{kd}^{rr} + i_{fd}^{rr} \right), \quad (11)$$

$$\lambda_{fd}^{rr} = L'_{lfd}i_{fd}^{rr} + k_{\text{sat}}^d L_{md} \left(-i_{ds}^r + i_{kd}^{rr} + i_{fd}^{rr} \right), \quad (12)$$

where: $L_{l\dots}$ represents the leakage inductances of the armature windings, $L'_{l\dots}$ represents the leakage inductances of the field and damper windings, L_{mq} and L_{md} are the magnetizing mutual inductances of the machine in the quadrature and direct axis, respectively, and k_{sat}^q and k_{sat}^d are the saturation coefficients of the machine in the quadrature and direct axis, respectively. The rated data of the studied SG and the identified equivalent circuit parameters can be found in Appendix. The parameter identification process was carried out based on data from the standstill frequency response (SSFR) test and the least-squares problem procedures [21, 22].

In general, the magnetic saturation effect in the salient pole machines can be different along the quadrature and direct axis, however, it can also be very similar. This depends highly on the construction of the machine, as well as the flux path, electric load type and saturation present in leakage inductances [20]. In non-salient pole machines (cylindrical type machines) the saturation along the direct and quadrature axis is similar. In this research, we assume that saturation affects the direct and quadrature axis in a similar way:

$$k_{\text{sat}}^q = k_{\text{sat}}^d \quad (13)$$

and the direct axis saturation coefficient is defined based on no-load machine characteristics as:

$$k_{\text{sat}}^d(i_m) = \frac{E_0(i_m)}{\omega_r i_m L_{sfd}}, \quad (14)$$

where: L_{sfd} is the mutual inductance between excitation and the field winding, E_0 is the no-load magnetizing back EMF (electromotive force) and the magnetizing current i_m is defined as:

$$i_m = \sqrt{\left(\frac{-i_{qs}^r + i_{kq}^{rr}}{k_{fd}} \right)^2 + \left(\frac{-i_{ds}^r + i_{kd}^{rr} + i_{fd}^{rr}}{k_{fd}} \right)^2}, \quad (15)$$

where the k_{fd} is a turn ratio coefficient between the armature winding and the field winding and can be calculated based on the number of turns of each winding or based on self and mutual inductances as:

$$k_{fd} = \frac{2 N_{fd}}{3 N_s} = \frac{L_{sfd}}{L_{md}}. \quad (16)$$

In steady-state no-load conditions' magnetizing current, i_m is equal to the excitation current $i_{fd}^r = i_{fd}^{rr}/k_{fd}$ (armature and damper winding currents are equal to 0). The mutual inductance L_{sfd} is also calculated using the no-load back EMF E_0 characteristic as:

$$L_{sfd} = \frac{E_0(i_{fd,0n}^r)}{\omega_r i_{fd,0n}^r}, \quad (17)$$

where $i_{fd,0n}^r$ is the excitation current of the SG that provides nominal armature voltage under no-load conditions.

The mechanical component of the SG electromechanical converter model is defined as:

$$T_l = T_e + B_m \omega_{rm} + J \frac{d\omega_{rm}}{dt}, \quad (18)$$

where: ω_{rm} is the mechanical rotational velocity of the machine and is equal to $\omega_{rm} = \omega_r / p$ (p – number of pole pairs of the SG), T_l is an external torque applied to the machine shaft, B_m is a coefficient accounting for the torque created due to mechanical losses (friction, aerodynamics and others), J is the SG and prime mover cumulative moment of inertia and T_e is the electromagnetic torque created in the machine and calculated as:

$$T_e = \frac{3p}{2} \left(\lambda_{ds}^r i_{qs}^r - \lambda_{qs}^r i_{ds}^r \right). \quad (19)$$

3. Developed model implementation

The developed model was implemented in the MATLAB/Simulink environment. A transformer-type IA was applied to the model for the PHIL emulation platform. In terms of the model output parameters, the armature RMS voltage value and armature voltage frequency are the set points used to control the FC output AC terminals. The armature RMS voltage value is calculated based on quadrature V_{qs} and direct V_{ds} armature voltage components as:

$$V_{AC} = \sqrt{\frac{1}{2} \left(V_{qs}^2 + V_{ds}^2 \right)}. \quad (20)$$

In addition to the functional level modelling approach, the assumption was that both the internal structure, as well as the terminal behaviour of the machine, are symmetrical. Based on that assumption the armature voltage is described using the values in quadrature and direct axes only. The zero component of the $qd0$ orthogonal arbitrary synchronous reference frame is not present in those conditions. In the MATLAB environment the armature voltage equations in quadrature (1) and direct (2) axes are defined as:

$$v_{qs} = -i_{qs} * r_s + \omega_{rm} * \text{phids} + D\text{phiqs}, \quad (21)$$

$$v_{ds} = -i_{ds} * r_s + \omega_{rm} * \text{phiqs} + D\text{phids}, \quad (22)$$

where the derivatives of quadrature (Dphiqs) and direct (Dphids) axes flux linkages over time are calculated in discrete form in MATLAB/Simulink as shown in Fig. 2.

In order to calculate the linkage flux and the voltage, the IA uses measured values of the output AC RMS current, as well as the active and reactive power components. The powers are used to calculate the power factor (PF) of the load connected to the terminals of the PHIL emulation platform. This is because the FC acquires and provides in real-time AC RMS current and active and reactive powers to the RTS. Such an approach introduces a certain delay due to the fact that to calculate RMS values historic data are required so the moving RMS calculation is employed.

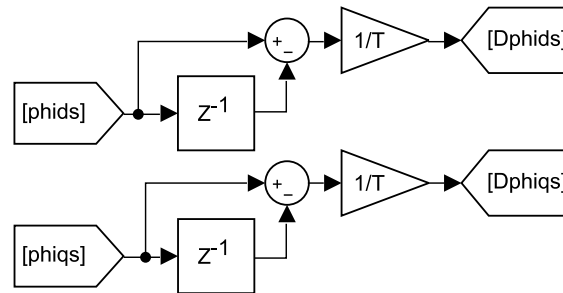


Fig. 2. Armature flux linkage derivative over the time calculation for quadrature and direct axes

In order to calculate input values of quadrature (i_{qs}) and direct (i_{ds}) axis currents both the phase shift angle between armature voltage and current waveforms (ϕ) and the load or torque angle (δ) need to be calculated.

The phase shift angle (ϕ) is calculated using the real-time value of the PF and the power angle (δ) is calculated using model output quadrature (V_{qs}) and direct (V_{ds}) axis voltages. Fig. 3 shows the phasor diagram of the SG under the load operation with both, the phase shift and delta angles indicated.

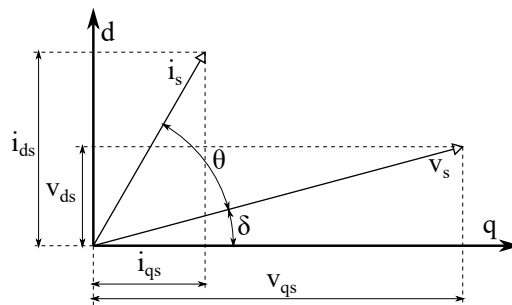


Fig. 3. Phasor diagram of SG under load operation - only armature voltage and current

Saturation coefficients in the quadrature k_{sat}^q and direct k_{sat}^d axis are calculated based on the no-load back EMF E_0 discrete characteristic implemented in the model in the form of a look-up table. The look-up table uses both linear interpolation and extrapolation of calculated EMF values. The measurements of no-load back EMF were performed for the excitation current value changing from near zero up to 1.7 times $i_{fd,0n}^r$. Figure 4 shows the MATLAB Simulink function for calculating the saturation coefficients. Parameters d_sat_en and q_sat_en are used for disabling the saturation coefficients calculation process and thus for not taking the saturation effects into account for comparison purposes.

The output frequency is calculated based on Eqs. (18) and (19) as:

$$f_{AC} = \frac{1}{p2\pi} \int \frac{T_l - T_e - B_m \omega_m}{J} dt \quad (23)$$



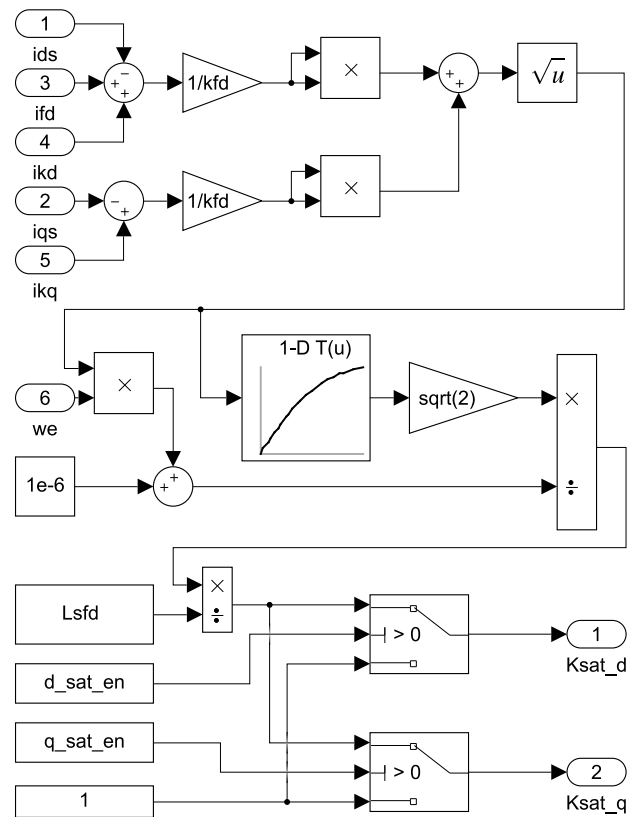


Fig. 4. MATLAB Simulink function for calculating the saturation coefficients

Figure 5 shows the MATLAB/Simulink implementation of the output frequency calculation.

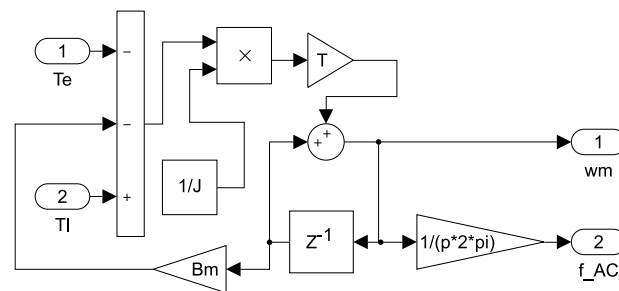


Fig. 5. PHIL emulation platform output AC voltage frequency calculation

The hardware under test (HUT) synchronous generator used for the PHIL validation was supplied with mechanical power (rotational velocity and external input torque) from the dynamometer test bench. This test bench was set to operate with constant velocity in steady-state conditions as

a diesel generator would. In order to replicate that with the PHIL emulation platform, a simple control algorithm was used to control the machine speed. Figure 6 shows the control loop for the prime mover torque T_I .

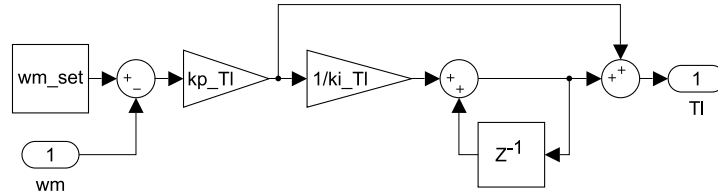


Fig. 6. Prime mover input torque estimation from the dynamometer test bench

4. Developed emulation platform validation

The PHIL hardware platform consisted of three main groups of components: Functional Units, Functional Unit Controllers, and Communication and control peripherals. The performance of a synchronous generator operating in an autonomous power system was emulated by the 150 kVA bidirectional DC/AC converter (Functional Unit II (FU II)). The FU II was the single source of energy with regulated voltage amplitude and frequency. It was connected to another power converter (FU I) which emulated passive active and/or reactive loads seen by the generator. The FU II was powered by a 650 V DC bus by a third converter (FU III) present in the investigated scenario. The FU III was fed from the main AC bus with 400 V. The simplified connection diagram is presented in Fig. 7.

The functional units were supervised by the Functional Unit Controllers (FUCs), marked as 2 in Fig. 7. The FUC includes an x64 Target PC rack-mounted in a 19" enclosure. The Target PC

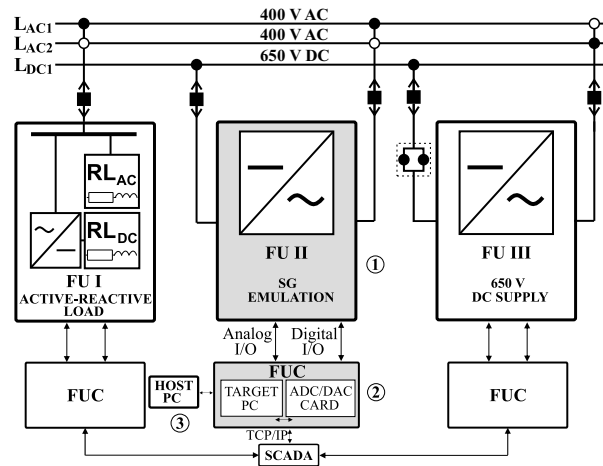


Fig. 7. Diagram of the functional units (FU marked as 1), functional unit controllers (FUC marked as 2), and communication and control peripherals (marked as 3) used in the emulation of the synchronous generator model



is governed by the Simulink Real-Time kernel which implements the real-time control algorithm and interfaces with the power converter by a measurement and control card (ADC/DAC CARD in Fig. 7). This enables required analog and digital inputs for measuring electrical quantities of the converter to be acquired by the Target PC. Binary states informing about the present status of the unit are monitored. Analogue and digital outputs that send the set-point values of AC voltage, frequency, and work-mode into the converter are also provided. The host PC, marked as 3 in Fig. 7, is used for development and control duties through the Simulink environment, while the SCADA allows control over the whole power system.

Measurements of the SG were performed using a dynamometer test bench depicted in Fig. 8. The drive motor of the test bench was operating with a rotation speed control loop, using torque and speed sensors as feedback. The armature and field windings' voltages and currents and the dynamometer torque and speed signals were acquired using the ZES ZIMMER LMG600 series multichannel power analyser. The excitation winding of the SG was supplied from a 36 V DC lead-acid battery (three 12 V batteries in series). Additional resistor R_{add} was used to set the current for nominal no-load voltage. The electrical load was provided by a 100 kW (at 400 V line to line) resistor and a 100 kvar (at 400 V line to line and 50 Hz) inductive load. Both of those load components were adjustable with 10% increments and are denoted in Fig. 8 as the impedance Z .

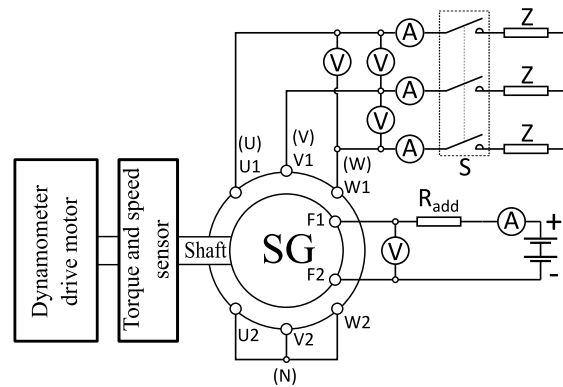


Fig. 8. Diagram of the measurement system used for the verification of the PHIL platform

The power electronics, real-time simulators, and the dynamometer test bench used in this research are part of the LINTE² laboratory of the Gdańsk University of Technology (Poland). The view of the main laboratory hall is presented in Fig. 9. The validation of the proposed approach was performed using experimental results of the transient and steady-state of a step change in SG load from no-load to selected load conditions. During the measurements, the generator operated at constant speed and constant excitation current under steady-state conditions.

Figure 10 shows the results of one of the performed load connection tests (switch-on of 90 kW active and 20 kvar reactive load). Both the voltage and current waveforms are shown for the SG measurements and the results from the PHIL emulator with and without the saturation effect are incorporated into the real-time simulation model. One can observe that the armature reaction demagnetizing effect is causing the core of the machine to be operating at different saturation levels in steady-state conditions. To illustrate this phenomenon, an automatic voltage regulator (AVR) was not used in the measured and emulated SG.

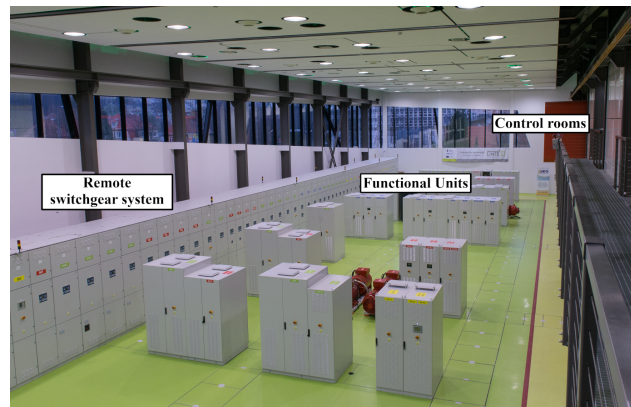
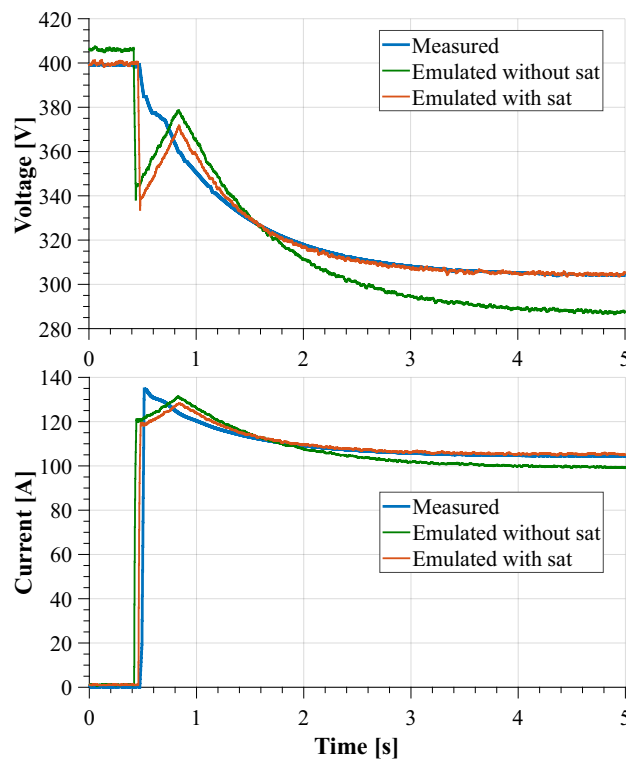
Fig. 9. LINTE² laboratory main hall

Fig. 10. Comparison of the measured and emulated armature voltage (upper graph) and current (lower graph) of the synchronous generator during a switch-on of 90 kW + 20 kvar

The specific load point was chosen from the load range of 10–100 kW with or without additional 20 kvar, to emphasise the different saturation levels of the SG and their effects on the armature voltage.

Figure 11 shows the calculated real-time simulation value of the direct axis saturation coefficient k_{sat}^d . We can see that this value changes not only under steady-state conditions but also in the transient state affecting the dynamic performance of the machine as well as the steady-state performance. Figure 12 presents the excitation current of the synchronous generator during switch-on. The calculated excitation current can be used as a signal for SG automatic voltage regulator (AVR) or the power management system (PMS) development.

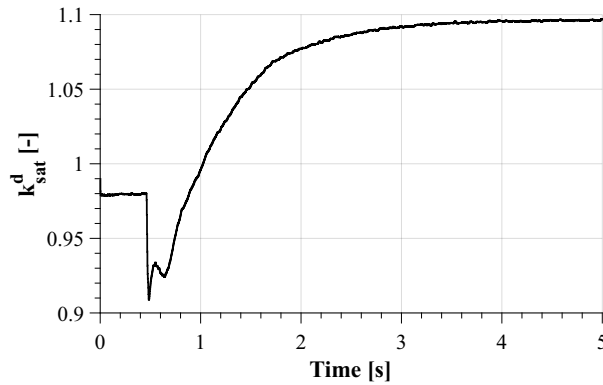


Fig. 11. Real-time simulation value of direct axis saturation coefficients k_{sat}^d

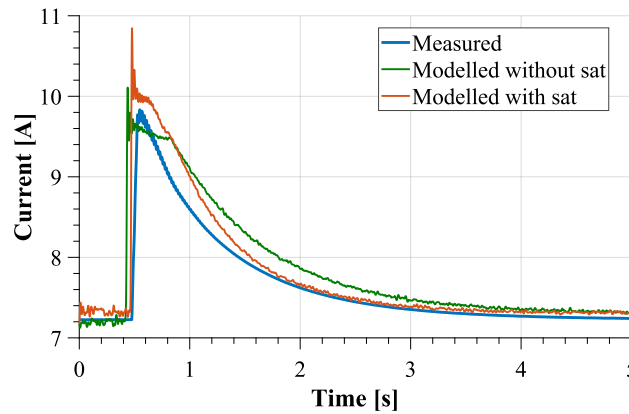


Fig. 12. Comparison of the measured and modelled real-time values of the excitation current of the synchronous generator during a switch-on of 90 kW + 20 kvar

In order to validate the proposed approach, a series of measurements were performed for different active and reactive load components. Figure 13 and Fig. 14 show the difference between SG measurements and the emulation platform measurements of the output voltages' values in the steady-state phase of the voltage waveform for different active and reactive loads applied.

The ΔV [%] was calculated according to:

$$\Delta V(t = 5 \text{ s}) = \frac{V_{\text{measured}} - V_{\text{emulated}}}{V_{\text{measured}}} \cdot 100\%, \quad (24)$$

where: V_{measured} is the steady state armature voltage for a given load of the SG, V_{emulated} is the emulated steady state inverter voltage for the respective load.

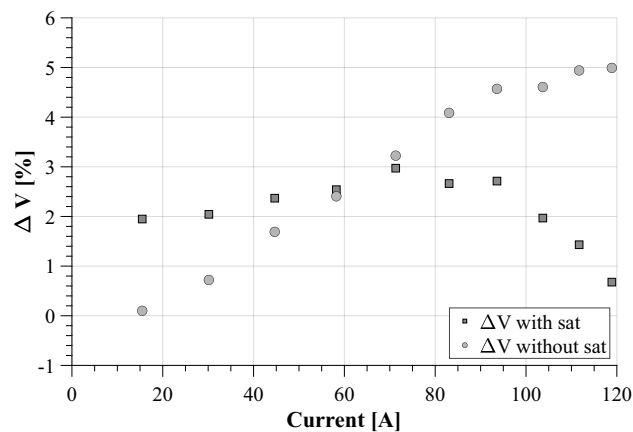


Fig. 13. Difference between measured and emulated armature steady-state voltage of synchronous generator during switch-on of active loads. Square markers indicate ΔV with included saturation effects, while cross markers indicate ΔV for the model without saturation effects

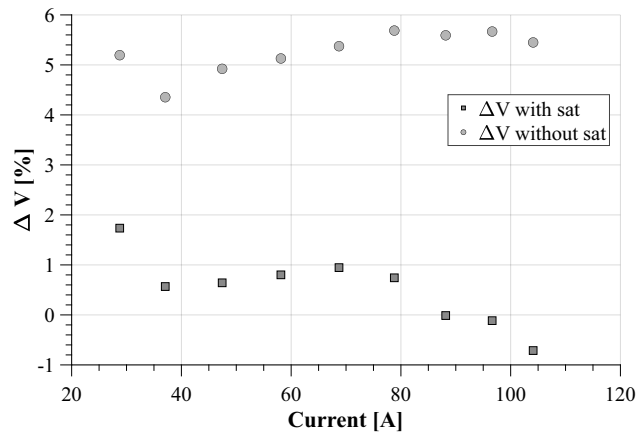


Fig. 14. Difference between measured and emulated armature steady-state voltage of synchronous generator during switch-on of active-reactive loads. Square markers indicate ΔV with included saturation effects, while cross markers indicate ΔV for the model without saturation effects



Figure 15 shows the frequency and mechanical torque of both the SG and the developed emulation platform. The main influence of the saturation effect in the model controlling the emulation platform is the accurate value of the torque under steady-state operation. In the case of the emulation platform, the torque is calculated in the model value, while with the SG it is the actual mechanical torque measured using a torque sensor (Fig. 8).

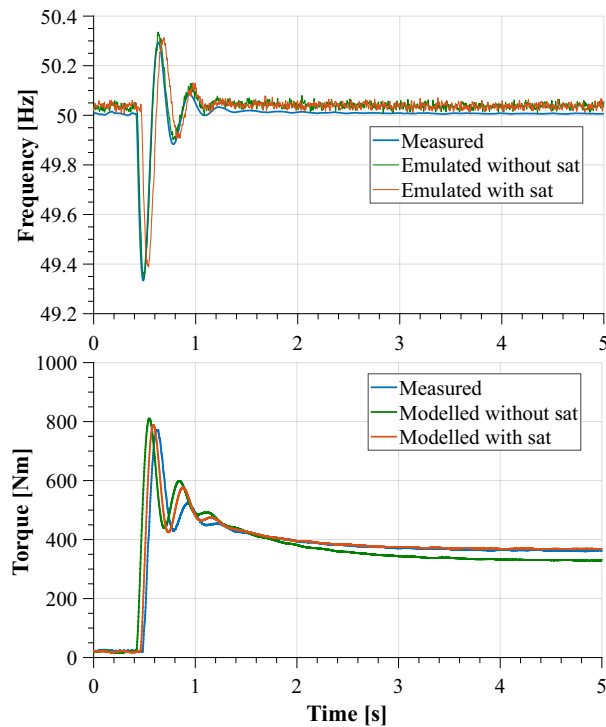


Fig. 15. Comparison of the measured and emulated frequency (upper graph) and measured and modelled torque (lower graph) of the synchronous generator during a switch-on of 90 kW + 20 kvar

5. Conclusions

The research presented in the paper focuses on the PHIL emulation platform development. The main objective of the studies was to validate the proposed approach of using a commercial-grade frequency converter as the power amplifier of the emulation platform. Such an approach enables autonomous power system studies at a reduced cost and decreased time of implementation compared to other PHIL platforms. A comparison of main advantages and disadvantages of such PHIL platforms is located in Table 1.

A synchronous generator model in an arbitrary synchronous reference frame was used in the real-time simulation. The model included the magnetic saturation effect to accurately represent the generator behaviour during sudden load changes. The proposed emulation platform requires

Table 1. Pros and cons of selected PHIL solutions

Presented platform	Turn-key PHIL solution	Dedicated power amplifier platform
Lowest price per kVA	Highest price per kVA	High price per kVA
Short time of implementation	Shortest time of implementation	Longest time of implementation
Lower precision of results	High precision of results	High precision of results

several hardware and software components to be replicated. In terms of software, a Simulink Real-time numerical model of an SG without algebraic loops is required. A voltage converter needs to be set-up for external control with set points for RMS voltage and frequency, which are computed by the Simulink model. In terms of hardware, the converter with accompanying filters needs to support fast enough current dynamics to follow the behaviour of the model. Moreover, an ADC/DAC interface card is needed with a minimal 12-bit resolution and a number of channels for measuring three-phase voltages, currents and operating frequency of the converter. The host x64 PC is required with computing power adequate for real-time execution of the model (under 1ms in our case). Finally, to test the performance of the platform, an active and/or passive load of suitable power rating is necessary. Due to the presence of an output filter in the frequency converter, the dynamic response of the proposed emulation platform is not accurate during 0.4 s of the initial transient state.

However, apart from that initial inaccuracy, the inclusion of the saturation effect improves significantly the performance of the proposed emulation platform. Moreover, the effect of saturation in the q -axis on the armature voltage of the generator presented in the research on active and reactive load conditions is negligible.

Appendix

Synchronous generator Elmor GCh114o/4 rated data:

- Frequency: $f_n = 50$ Hz,
- Voltage: $U_n = 400$ V,
- Power: $S_n = 125$ kVA,
- Current: $I_n = 180$ A,
- Power factor: $PF = 0.8$.

Identified equivalent circuits' parameters in SI units of the Elmor GCh114o/4 synchronous generator seen from the stator side:

- $L_{sfd} = 0.144$ H,
- $L_{ls} = 0.4e - 3$ H,
- $L_{md} = 3.8e - 3$ H,
- $L_{mq} = 2.8e - 3$ H,
- $L_{lkd} = 0.2e - 3$ H,
- $L_{lkq} = 0.1e - 3$ H,
- $L_{lfd} = 0.21e - 3$ H,

- $r_s = 33e - 3 \Omega$,
- $r_{fd} = 2.3e - 3 \Omega$,
- $r_{kd} = 0.3 \Omega$,
- $r_{kq} = 0.8 \Omega$.

Base values:

- Frequency: $f_b = f_n = 50$ Hz,
 Pulsation: $\omega_b = 2\pi f_b = 314.1593$ rad/s,
 Impedance: $Z_b = U_{n2}/S_n = 1.28 \Omega$,
 Inductance: $L_b = Z_b/\omega_b = 0.0041$ H.

References

- [1] Nadarajan S., Panda S.K., Bhangu B., Gupta A.K., *Online Model-Based Condition Monitoring for Brushless Wound-Field Synchronous Generator to Detect and Diagnose Stator Windings Turn-to-Turn Shorts Using Extended Kalman Filter*, IEEE Transactions on Industrial Electronics, vol. 63, no. 5, pp. 3228–3241 (2016), DOI: [10.1109/TIE.2016.2535959](https://doi.org/10.1109/TIE.2016.2535959).
- [2] Racewicz S., Kutt F., Sienkiewicz Ł., *Power Hardware-In-the-Loop Approach for Autonomous Power Generation System Analysis*, Energies 2022, vol. 15, no. 5, p. 1720 (2022), DOI: [10.3390/en15051720](https://doi.org/10.3390/en15051720).
- [3] Kumar D., Zare F., *A Comprehensive Review of Maritime Microgrids: System Architectures, Energy Efficiency, Power Quality, and Regulations*, IEEE Access, vol. 7, pp. 67249–67277 (2019), DOI: [10.1109/ACCESS.2019.2917082](https://doi.org/10.1109/ACCESS.2019.2917082).
- [4] Noon J., Song H., Wen B., Burgos R., Cvetkovic I., Boroyevich D., Srdic S., Pammer G., *A Power Hardware-in-the-Loop Test bench for Aerospace Applications*, Conference Proceedings – IEEE Applied Power Electronics Conference and Exposition – APEC, vol. 2020-March, pp. 2884–2891 (2020), DOI: [10.1109/APEC39645.2020.9124299](https://doi.org/10.1109/APEC39645.2020.9124299).
- [5] Faizan Shaikh M., Kim H.J., Lee S.B., Lim C., *Online Airgap Flux Based Diagnosis of Rotor Eccentricity and Field Winding Turn Insulation Faults in Synchronous Generators*, IEEE Transactions on Energy Conversion, vol. 37, no. 1 (2022), DOI: [10.1109/TEC.2021.3092198](https://doi.org/10.1109/TEC.2021.3092198).
- [6] Lauss G., Feng Z., Syed M.H., Kontou A., Paola A.D., Paspatis A., Kotsampopoulos P., *A Framework for Sensitivity Analysis of Real-Time Power Hardware-in-the-Loop (PHIL) Systems*, IEEE Access, vol. 10, pp. 101305–101318 (2022), DOI: [10.1109/ACCESS.2022.3206780](https://doi.org/10.1109/ACCESS.2022.3206780).
- [7] Jhuma U.K., Mekhilef S., Ahmad S., Islam J., Jesan J.R., Billah M.M., *The Impact of Synchronous Generator on Voltage Sag Mitigation in Power System Network*, 2021 IEEE 4th International Conference on Computing, Power and Communication Technologies, GUCON 2021 (2021), DOI: [10.1109/GUCON50781.2021.9573961](https://doi.org/10.1109/GUCON50781.2021.9573961).
- [8] Monieta J., Nowicki M., *Experimental manners of an interference reduction of chosen measuring signals of a generating set in conditions of a marine power plants*, Diagnostyka, vol. 19, no. 1, pp. 93–102 (2018), DOI: [10.29354/diag/82975](https://doi.org/10.29354/diag/82975).
- [9] Lee J.S., Choi G., *Modeling and hardware-in-the-loop system realization of electric machine drives — A review*, CES Transactions on Electrical Machines and Systems, vol. 5, no. 3, pp. 194–201 (2021), DOI: [10.30941/CESTEMS.2021.00023](https://doi.org/10.30941/CESTEMS.2021.00023).
- [10] Lundstrom B., Salapaka M.V., *Optimal Power Hardware-in-the-Loop Interfacing: Applying Modern Control for Design and Verification of High-Accuracy Interfaces*, IEEE Transactions on Industrial Electronics, vol. 68, no. 11, pp. 10388–10399 (2021), DOI: [10.1109/TIE.2020.3032918](https://doi.org/10.1109/TIE.2020.3032918).
- [11] Hong Q., Abdulhadi I., Tzelepis D., Roscoe A., Marshall B., Booth C., *Realization of High Fidelity Power-Hardware-in-the-Loop Capability Using a MW-Scale Motor-Generator Set*, IEEE Transactions on Industrial Electronics, vol. 67, no. 8, pp. 6835–6844 (2020), DOI: [10.1109/TIE.2019.2937038](https://doi.org/10.1109/TIE.2019.2937038).

- [12] Lauss G., Strunz K., *Accurate and Stable Hardware-in-the-Loop (HIL) Real-Time Simulation of Integrated Power Electronics and Power Systems*, IEEE Transactions on Power Electronics, vol. 36, no. 9, pp. 10920–10932 (2021), DOI: [10.1109/TPEL.2020.3040071](https://doi.org/10.1109/TPEL.2020.3040071)
- [13] Lauss G.F., Faruque M.O., Schoder K., Dufour C., Viehweider A., Langston J., *Characteristics and design of power hardware-in-the-loop simulations for electrical power systems*, IEEE Transactions on Industrial Electronics, vol. 63, no. 1, pp. 406–417 (2016), DOI: [10.1109/TIE.2015.2464308](https://doi.org/10.1109/TIE.2015.2464308).
- [14] Lehfuss F., Lauss G., Kotsampopoulos P., Hatzigiargyriou N., Crolla P., Roscoe A., *Comparison of multiple power amplification types for power Hardware-in-the-Loop applications*, 2012 IEEE Workshop on Complexity in Engineering, COMPENG 2012 – Proceedings, pp. 95–100 (2012), DOI: [10.1109/CompEng.2012.6242959](https://doi.org/10.1109/CompEng.2012.6242959).
- [15] Yang L., Wang J., Ma Y., Wang J., Zhang X., Tolbert L.M., Wang F.F., Tomsovic K., *Three-Phase Power Converter-Based Real-Time Synchronous Generator Emulation*, IEEE Transactions on Power Electronics, vol. 32, no. 2, pp. 1651–1665 (2017), DOI: [10.1109/TPEL.2016.2553168](https://doi.org/10.1109/TPEL.2016.2553168).
- [16] Rosenberger R., Huss S.A., *A systems theoretic approach to behavioural modeling and simulation of analog functional blocks*, Proceedings – Design, Automation and Test in Europe, DATE, pp. 721–728 (1998), DOI: [10.1109/DATE.1998.655938](https://doi.org/10.1109/DATE.1998.655938).
- [17] Jomier T., *Technical Report (MOET-FP6-030861)*, Tech. Rep., AIRBUS OPERATIONS S.A.S. (2009).
- [18] Ashourianjozdani M., Lopes L.A., Pillay P., *Power electronic converter based pmsg emulator: A testbed for renewable energy experiments*, IEEE Transactions on Industry Applications, vol. 54, pp. 3626–3636 (2018), DOI: [10.1109/TIA.2018.2819618](https://doi.org/10.1109/TIA.2018.2819618)
- [19] El-Sousy F.F.M., Aziz G.A.A., Amin M., Gaber K., Mohammed O.A., *A high-speed microturbine pma-synrg emulation using power hardware-in-the-loop for wind energy conversion systems*, IEEE Access, vol. 8, pp. 194612–194622 (2020), DOI: [10.1109/ACCESS.2020.3033485](https://doi.org/10.1109/ACCESS.2020.3033485).
- [20] Kar N.C., El-Serafi A.M., *Measurement of the saturation characteristics in the quadrature axis of synchronous machines*, IEEE Transactions on Energy Conversion, vol. 21, no. 3, pp. 690–698 (2006), DOI: [10.1109/TEC.2006.877368](https://doi.org/10.1109/TEC.2006.877368).
- [21] IEEE Std 115-1995, 115-2009 – *IEEE Guide for Test Procedures for Synchronous Machines Part I – Acceptance and Performance Testing Part II – Test Procedures and Parameter Determination for Dynamic Analysis*, IEEE: New York, NY, USA (2010), DOI: [10.1109/IEEESTD.2020.9020274](https://doi.org/10.1109/IEEESTD.2020.9020274).
- [22] Racewicz S., Kutt F., Michna M., Sienkiewicz Ł., *Comparative Study of Integer and Non-Integer Order Models of Synchronous Generator*, Energies, vol. 13, no. 17, 4416 (2020), DOI: [10.3390/en13174416](https://doi.org/10.3390/en13174416).

